PCCP

ROYAL SOCIETY OF CHEMISTRY

PAPER

View Article Online
View Journal | View Issue

Check for updates

Cite this: *Phys. Chem. Chem. Phys.*, 2026, **28**, 8847

Probing sulfur-centered intra- and intermolecular interactions in mercaptoethanol from the gas to liquid phase: a raman spectroscopic and theoretical study

Siyao Li,[a] Yuhui Li,[b] Xinlang Yang,[b] Yuanqin Yu, *[a] Xiaoguo Zhou, [b] Rui Zhang,[a] Jinsong Li[a] and Shilin Liu *[b]

Received 3rd February 2026,
Accepted 6th March 2026

DOI: 10.1039/d6cp00389c

rsc.li/pccp

Sulfur-centered hydrogen bonding plays an important yet insufficiently understood role in molecular structure and intermolecular interactions due to the relatively low electronegativity of sulfur. Mercaptoethanol ($HSCH_2CH_2OH$, ME), containing both S–H and O–H functional groups, serves as an ideal prototype for examining sulfur-involved hydrogen bonds in different environments. In this work, high-resolution gas-phase Raman spectra of ME were recorded in the S–H stretching region using stimulated photoacoustic Raman spectroscopy and analyzed in conjunction with quantum chemical calculations and temperature-dependent measurements. Comparison between experimental and simulated spectra enables an unambiguous assignment of individual Raman bands to specific conformers and reveals that *gauche* conformers stabilized by O–H···S intramolecular hydrogen bonds dominate in the gas phase, while S–H···O intramolecular interactions are present but extremely weak. In contrast, liquid-phase Raman spectra exhibit a red shift of the S–H stretching band in neat mercaptoethanol relative to that in an aqueous solution. Quantum chemical calculations on ME–ME and ME–H_2O dimers demonstrate that this red shift originates from a significantly enhanced S–H···O intermolecular hydrogen bond in the liquid state. These results provide direct spectroscopic evidence for the environment-dependent nature of sulfur-centered hydrogen bonding and offer molecular-level insights into the interplay between intramolecular and intermolecular interactions involving sulfur.

1. Introduction

Weak intermolecular forces are prevalent in nature and determine molecular conformations and molecular packing arrangements in crystals. Hydrogen bonds (H-bonds) are the most common weak interactions in molecules and have been the center of attention for many experimental and theoretical studies. Besides their ubiquitous presence, hydrogen bonds play a dominant role in solute–solvent interactions and the physical and chemical properties of the solvents, and most importantly, in regulating the specific structures and functions of biological macromolecules such as proteins and nucleic acids.[1,2] Generally, hydrogen bonds can be represented as X–H···Y, where X is the hydrogen-bond donor and Y is the hydrogen-bond acceptor, both of which are atoms with high electronegativity (such as O and N). Conventional hydrogen bonds, such as O–H···O, O–H···N, and N–H···O, whether intramolecular or intermolecular interactions, have been extensively studied and characterized in the literature.[3–8] In contrast, insufficient attention has been paid to unconventional H-bonds involving sulfur, which has lower electronegativity. The electronegativity of sulfur (2.58) is significantly lower than that of oxygen (3.44) and nitrogen (3.04), and the difference in electronegativity between sulfur and hydrogen is very small, $\Delta \sim 0.38$ on the Pauling scale. This leads to the general belief that sulfur is not an effective participant in H-bonds. However, the role of the sulfur-centered H-bond is clear because of its biological and environmental importance.[9,10] For example, sulfur-containing amino acids, such as cysteine and methionine, are the basic building blocks of proteins. Sulfur participates in the formation of the spatial structure of proteins through disulfide bonds (–S–S–); this is crucial for maintaining the stability of the protein structure, and the biological activity of many proteins (such as insulin) also depends on the correct disulfide bond connectivity.[11–14] Therefore, a deeper understanding of the nature of sulfur-centered H-bonds is of great significance for regulating the reactivity of biomolecules, designing sulfur-containing supramolecular assemblies, and developing drugs.

[a] *School of Physics, Anhui University, Hefei, 230601, China. E-mail: yyq@ahu.edu.cn*
[b] *Department of Chemical Physics, Hefei National Research Center of Physical Sciences at the Microscale, Hefei National Laboratory, University of Science and Technology of China, Hefei 230026, China. E-mail: slliu@ustc.edu.cn*

In recent years, there has been a growing interest in investigating sulfur-centered intermolecular H-bonds in binary complexes formed under supersonic jet-cooled conditions, especially in the case of sulfur acting as a H-bond donor, *e.g.*, S–H···S, S–H···O, S–H···π and S–H···Cl.[15–31] It has been shown that the sulfur-centered intermolecular H-bonds could be as strong as conventional H-bonds under certain conditions. For example, using a synergic experimental–computational approach from microwave spectroscopy, infrared laser spectroscopy and quantum chemical calculations, the formation of the elusive S–H···S H-bond and the competition between S–H···O, O–H···S and O–H···O interactions have been recently explored in pure and mixed dimer structures of 2-phenylethanethiol (PET) and 2-phenylethanol (PEAL).[20] Very recently, the weak C–H···S interaction has been identified in binary complexes such as $CHCl_3$–H_2S and diethyl disulfide-difluoromethane.[23,24,27] While rich information has been obtained on the sulfur-centered intermolecular interactions in the jet-cooled complex, the exploration of intramolecular interactions in the gas-phase monomers or intermolecular interactions in the condensed phase is still limited[32,33] and further molecular-level research is needed.

The gas phase provides an environment for the observation of specific weak intramolecular interactions, which would otherwise be blurred in the complexes or in the condensed media. Recently, gas-phase Raman spectroscopy coupled with quantum chemistry calculations has been demonstrated very effectively in characterizing molecular structures and intramolecular interactions.[34–37] Because of the sharpness of Raman bands in a gas-phase environment compared to infrared spectroscopy, it is easier to identify specific conformations from well-separated Raman bands and correlate the stability of the conformers with intramolecular interaction strength. When the isolated molecules are well characterized, the obtained information can then be used to evaluate the effects of intermolecular interactions on molecular structures and intramolecular interactions.

In previous studies, intramolecular interactions in the gas phase have been revealed in several 1,2-disubsituted ethanes, such as aminoethanol ($NH_2CH_2CH_2OH$), which exhibits both O–H···N and N–H···O intramolecular H-bonds.[38–40] Mercaptoethanol ($HSCH_2CH_2OH$, ME) contains both S–H and O–H functional groups, providing the opportunity for the formation of O–H···S or S–H···O intramolecular H-bonds, analogous to the interactions in aminoethanol. The gas-phase measurements from overtone spectroscopy and microwave spectroscopy have shown that the ME molecule prefers a *gauche* arrangement stabilized by an O–H···S intramolecular H-bond with a lack of unambiguous structural information on the S–H···O interaction.[41,42] Incomplete infrared spectral data indicate the presence of *trans* and *gauche* conformations in the liquid state, with the former being more stable by 600 cal mol^{-1}.[43] With the S–H stretching vibration as a probe, this study was conducted to obtain further evidence of sulfur atoms participating in H-bonding interactions in gaseous and liquid ME, especially the possibility of sulfur atoms acting as H-bond donors, using stimulated photoacoustic Raman spectroscopy and conventional Raman spectroscopy, as well as quantum chemistry calculations, respectively. It was also expected that the results would provide more basic information on the competition and synergism of sulfur-centered intramolecular and intermolecular interactions in different environments.

2. Experimental and theoretical methods

2.1 Experimental

The gas-phase Raman spectra were acquired using stimulated photoacoustic Raman spectroscopy (PARS), the details of which have been fully described elsewhere.[35–37] Briefly, a stimulated Raman scattering (SRS) process occurs when the frequency difference between two laser beams (pump and Stokes beams) equals a Raman-active vibrational mode, leading to the transitions of molecules from the ground state to the excited state. The collisions between molecules cause vibrational excitation energy to convert into local heating in the sample cell, which creates a sound wave detected by a sensitive microphone. The PARS method effectively overcomes the inherent low sensitivity of spontaneous Raman scattering in the gas phase.

In PARS, the second-harmonic output of 532.1 nm from a pulsed Nd : YAG laser (line width 1.0 cm^{-1}, pulse width 10 ns) is split into two laser beams by a quartz wedge; one is the pump beam and the other is the Stokes beam. About 10% of the laser energy was used as the pump beam, while the remainder directly entered a dye laser system (ND6000, line width 0.05 cm^{-1}) to generate a tunable Stokes beam (625–637 nm). The two laser beams were linearly polarized and focused in the center of a photoacoustic cell with a counterpropagating configuration. The PARS signal was averaged by a boxcar integrator and then input into a computer to acquire the Raman spectrum. The pump and Stokes beams are typically 20 and 10 mJ per pulse, respectively. The intensity of the final spectrum is normalized relative to that of the Stokes beam. The wavelengths of laser beams were calibrated by a wavelength meter with an accuracy of 0.005 nm.

The mercaptoethanol (ME) used in this study was purchased from Aladdin with spectroscopic grade purity (99%). To avoid interference from water signals, ME was dried using 3 Å molecular sieves before use. The dried sample was then sealed in a glass tube connected to a vacuum line and degassed through multiple freeze–pump–thaw cycles. To remove residual water vapor as thoroughly as possible, the sample cell was heated under vacuum for approximately two hours. Due to the low saturated vapor pressure of ME, about 20 Torr of argon was introduced into the photoacoustic cell as a buffer gas to enhance the photoacoustic signal intensity. For temperature-dependent spectral measurements, the entire photoacoustic cell was wrapped with a 500 W heating tape. The temperature was maintained below 65 °C due to the response limitations of the microphone used.

Liquid Raman spectra were recorded on a conventional Raman spectrometer as follows.[8,44] A 532 nm laser from Coherent Verdi (5 W) was used as the excitation source and the Raman scattering photons were collected by a pair of quartz lenses of f = 2.5 and 10 cm with a 180° back-scattering

configuration, which were imaged onto the entrance slit of a triple monochromator (Acton Research, TriplePro) equipped with a liquid nitrogen cooled CCD array (Princeton Instruments, Spec-10 : 100B). The final spectrum was an average of 15 single scans and the typical exposure time was about 2 s. A 600 groove mm^{-1} grating was used. To achieve the desired molar fraction of ME in water, the ME and water were prepared by measuring their respective volumes.

2.2 Computational details

All gas-phase calculations were done using the Gaussian 16 suite of programs,[45] including geometry optimizations, zero-point energy (ZPE), and harmonic vibrational frequencies. The initial conformation was investigated using a semi-empirical method of PM7 based on the Molclus code[46] in which an energy threshold of 0.25 kcal mol^{-1} was applied, and then the low-energy conformations were further optimized at B3LYP-D3(BJ) functionals with the aug-cc-pVDZ or 6-311++G(d,p) basis set. In previous studies, B3LYP-D3(BJ) was demonstrated to perform well in predicting molecular structures containing intramolecular and intermolecular interactions.[25,47] To get more accurate relative energies in the gas phase, the single-point energies were calculated at the CCSD(T)/aug-cc-PVTZ level. To assist the assignment of experimental spectra, the intensity of the simulated Raman spectra was obtained by the Raman activities (S_i) and depolarization ratios (ρ_i), as well as the Boltzmann factors of each conformer according to the following equation:

$$I_i = \frac{F(\nu_0 - \nu_i)^4 S_i}{\nu_i(1+\rho_i)[1-\exp(-hc\nu_i/kT)]} \quad (1)$$

where υ_0 is the excitation energy in cm^{-1}, and I_i and υ_i are the Raman intensity and vibrational frequency (cm^{-1}) of the ith normal mode, respectively, T is the temperature, h and k are Planck's and Boltzmann's constants, and F is the Boltzmann factor for the population of each conformer. The Boltzmann factors were determined by the Gibbs free energy (ΔG) using the Shermo program (version 2.3.5) at the CCSD(T)/aug-cc-PVTZ level with zero-point energy (ZPE) correction at the B3LYP-D3(BJ)/aug-cc-PVDZ level.[48] The following expression was used:

$$F_i = \frac{\exp(-\Delta G_i/RT)}{\sum \exp(-\Delta G_i/RT)} \times 100\% \quad (2)$$

where ΔG_i is the relative free energy of conformer "i" with respect to the lowest energy conformer and R = 0.00199 kcal $(mol\ K)^{-1}$ is the Boltzmann constant.

Intramolecular interactions were characterized using non-covalent interaction (NCI) theory, a topological method based on electron density.[49] In the NCI approach, the electron density $\rho(r)$ was multiplied by the sign of the second Hessian eigenvalue (λ_2) to identify the type of weak interaction. The results were then visualized by mapping the color-coded area according to the values of sign(λ_2) × $\rho(r)$. Here, the blue, green and red represent strong attractive, weaker, and repulsive interactions, respectively. NCI analyses were carried out using the Multiwfn program and visualized using the VMD software (version 1.9.3).[50]

3. Results and discussion

3.1 Calculated structures and intramolecular interactions

Owing to the three dihedral angles of H–S–C–C, S–C–C–O, and C–C–O–H, mercaptoethanol (ME) exhibits a rich conformational distribution, giving 13 distinct conformers. Fig. 1 presents the optimized structures of the selected ten lowest-energy conformers at the B3LYP-D3(BJ)/aug-cc-PVDZ level, together with the NCI analysis for the first five conformers. The structural parameters in Fig. 1 are consistent with those from other *ab initio* calculations, such as at the MP2/aug-cc-PV(D+T)Z level.[42] The following notation is used for conformational description: capital letters T and G denote the backbone dihedral angles of H–S–C–C and S–C–C–O, while lowercase letters g and t specify the C–C–O–H dihedral angle. Here, T and t correspond to a *trans* conformation (~180°), whereas G and g represent a *gauche* arrangement of about +60; the prime symbol (′) indicates a negative value of the corresponding dihedral angle. Table 1 lists the calculated relative energies and Boltzmann factors of the ten conformers. The most stable conformer 1 of GGg accounts for almost half of the population at room temperature.

As shown in Fig. 1(a), all the first four lowest-energy conformers adopt a *gauche* arrangement of the O–C–C–S backbone. Among them, conformers 1 and 2 (GGg and G′Gg) exhibit an O–H···S interaction with H···S distances of 2.64 Å and 2.79 Å, respectively, while conformers 3 and 4 (G′Gt and G′Gg′) display an S–H···O interaction with H···O distances of 2.59 Å and 2.57 Å, respectively. The subsequent conformers 5, 6, and 7 have an O-C-C-S dihedral angle close to 180°, corresponding to a *trans* configuration without intramolecular interactions. For a hydrogen bond to form, the distance between the proton and the proton acceptor must be less than the sum of their van der Waals radii. According to Pauling's calculations, the commonly accepted sum of van der Waals radii for H and O atoms is 2.60 Å, and that for H and S atoms is 3.05 Å.[42]

Table 2 summarizes the calculated O–H···S and S–H···O distances in conformers 1-4, along with their deviation (Δ) from the sums of the corresponding van der Waals radii. It can be seen that the O–H···S distances in conformers 1 and 2 are shorter than 3.05 Å by 0.41 Å and 0.26 Å, respectively. This indicates that both conformers are stabilized by an O–H···S intramolecular hydrogen bond, although the latter is significantly weaker than the former due to the deviation of the O–H bond from the lone-pair direction of the S atom, as shown in Fig. 1(a). The more diffuse distribution of the lone-pair electrons on sulfur provides some flexibility in H-bond formation, which partially compensates for the unfavorable geometry in conformer 2. For conformers 3 and 4, the calculated S–H···O distances are only 0.01 Å and 0.03 Å shorter than the sum of the van der Waals radii (2.60 Å), implying that these two conformers possess only a very weak, marginal S–H···O intramolecular interaction. All these structural features point to intramolecular hydrogen bonding as the important stabilizing factor governing the conformational arrangement of ME. This is consistent with the calculated Boltzmann factors (Table 1), which show that conformers 1–4 have significantly higher populations than the *trans* conformers.

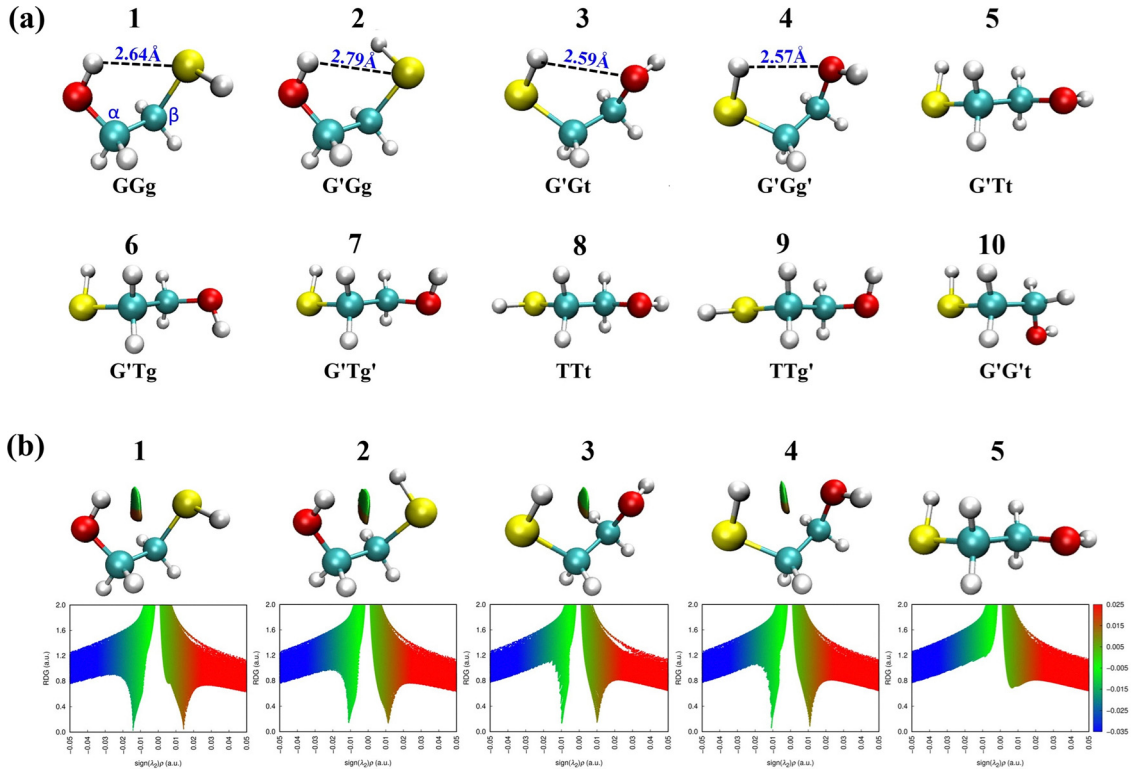

Fig. 1 (a) Optimized geometries of ten conformers of ME at the B3LYP-D3(BJ)/aug-cc-PVDZ levels. (b) NCI analysis for the first five conformers of ME. The nomenclature of the conformers: the uppercase letters (G and T) refer to the orientation of the backbone dihedral angles of H–S–C–C and S–C–C–O, the lowercase letters refer to the orientation of C–C–S–H, and the prime (′) indicates a negative value of the corresponding dihedral angle.

In Fig. 1(b), the NCI analysis confirms the presence of O–H···S and S–H···O interactions in conformers 1–4, whereas for conformer 5, there are no intramolecular interactions. The representation of the reduced electronic density gradient *versus* the signed electronic density shows a minimum near −0.01 in the conformers 1–4, associated with the O–H···S and S–H···O interactions. The minimum corresponding to conformer 1 exhibits a more negative value (<−0.01), suggesting a larger strength of O–H···S compared to S–H···O. This means that the electronegativity of the donor is far more important than that of the acceptor for sulfur-centered H-bonds. This is in good agreement with the trend of conventional H-bonds such as O–H···N and N–H···O, in which the electronegativity of the donor plays a dominant role, making O–H···N stronger than N–H···O, as demonstrated in recent studies of aminoethanol.[40]

Table 1 Calculated relative energies ΔE (kcal mol^{-1}) and Boltzmann factors (F) for ten conformers of ME

Number	Conformer	ΔE^a	F (%)^b
1	GGg	0	49.91
2	G′Gg	0.44	23.70
3	G′Gt	1.01	9.01
4	G′Gg′	1.45	4.32
5	G′Tt	1.46	4.25
6	G′Tg	1.51	3.91
7	G′Tg′	1.53	3.76
8	TTt	2.61	0.61
9	TTg′	2.69	0.53
10	G′G′t	2.74	0.49

[a] Calculated at the CCSD(T)/aug-cc-PVTZ//B3LYP-D3(BJ)/aug-cc-PVDZ level. [b] Boltzmann populations obtained from Gibbs free energy (ΔG) calculated by CCSD(T)/aug-cc-PVTZ electronic energies with ZPE using B3LYP-D3(BJ)/aug-cc-PVDZ at 298 K.

3.2 Gas-phase raman spectra in the S–H stretching region

Fig. 2 presents the gas-phase Raman spectra of ME in the S–H stretching region at room temperature (25 °C). Three prominent Raman bands are observed at 2587, 2593, and 2601 cm^{-1}, with a weak shoulder discernible at 2604 cm^{-1}. To assign the observed bands to specific conformers, the calculated frequencies and Raman activities of each ME conformer were convolved with a Lorentzian function according to eqn (1) to produce the simulated S–H stretching Raman spectra, as shown in Fig. 2(b), while the contributions from individual conformers are labeled in Fig. 2(c). To match the experimental spectra, a scaling factor of 0.978 was applied to all the calculated harmonic frequencies by comparing with that of the most stable conformer. It can be seen that the overall profile of the simulated spectrum agrees well with the experimental spectrum, except for a deviation in the highest-frequency band of conformer 3.

A close comparison between experimental and simulated spectra allows us to assign the observed S–H stretching spectra, as summarized in Table 3, and labeled in Fig. 2. The strongest band at 2587 cm^{-1} corresponds to the most stable conformer 1 (GGg), the second band at 2595 cm^{-1} corresponds to the

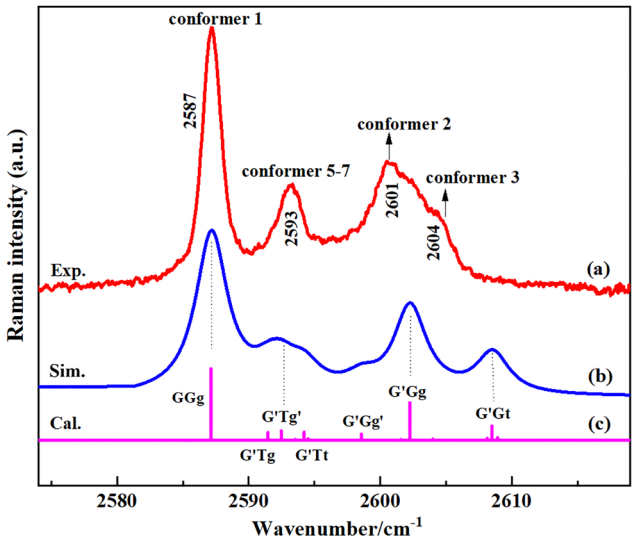

Fig. 2 (a) Gas-phase Raman spectra of ME in the S–H stretching region. (b) Simulated spectra for ME in the S–H stretching region according to eqn (1). (c) Calculated Raman intensities and frequencies for the individual conformers of ME.

superposition of conformers 5, 6 and 7 (G′Tg, G′Tt and G′Tg′), and the third band at 2601 cm^{-1} corresponds to conformer 2 (G′Gg). Comparing the band at 2601 cm^{-1} with the other two bands, it is obviously broader with a distinguishable shoulder at 2604 cm^{-1}, suggesting that this band likely arises from multiple conformers. Hence, we assign the shoulder at 2604 cm^{-1} to conformer 3 (G′Gt). This assignment is reasonable considering that the calculated Boltzmann factor of conformer 3 is as high as 9.01%, although its predicted position at 2609 cm^{-1} does not correspond well to the observed one at 2604 cm^{-1}. Conformer 4 (G′Gg′), however, cannot be clearly identified in the experiment owing to its lower population of 4.32% and the frequency being very close to that of conformer 2 (G′Gg).

It should be mentioned that the calculated Boltzmann factors for the *trans* conformers of 5, 6, and 7 are only 4.25%, 3.91%, and 3.76%, respectively, significantly lower than those of the *gauche* conformers. The reason they can still be detected is that they have close frequencies whose calculated values are 2593, 2595, and 2592 cm^{-1}, respectively, and thus their superposition gives rise to an observable band at 2593 cm^{-1}. Previous microwave-rotation studies failed to detect the *trans* conformers of 2-ME, which may be due to the lower dipole moments of *trans* conformers compared to the *gauche* conformers,[41] whereas in gas-phase infrared measurements, the failure could be attributed to spectral congestion.[42]

The H-bond formation generally leads to bond elongation and a red shift in the stretching frequency.[51] From the calculated structures, one would expect conformers 3 and 4 to exhibit a red shift in the S–H stretching frequency. However, as seen in Fig. 2, no such red shift is observed for the assigned conformer 3 relative to conformers 1 and 2. The reasons may be as follows. The S–H stretching frequency in ME conformers is influenced by two main factors: the spatial orientation of the S–H group and the strength of intramolecular interactions. Different

Table 2 Calculated H-bond distances (Å) along with their deviations Δ(Å) from the sum of van der Waals radii in the monomer conformers and dimers

		O–H···S		S–H···O		O–H···O	
Conformer		R(H···S)[a]	Δ[b]	R(H···O)[a]	Δ[b]	R(H···O)[a]	Δ[b]
ME	1	2.64	0.41				
	2	2.79	0.26				
	3			2.59	0.01		
	4			2.57	0.03		
ME–ME		2.39	0.66	2.21	0.39	1.83	0.77
ME–H_2O		2.39	0.66			1.89	0.71

[a] Calculated at B3LYP-D3(BJ)/aug-cc-PVDZ. [b] Δ denotes the deviation of the H-bond distance from the sum of the corresponding van der Waals radii. An intramolecular H-bond is expected to form if the H-bond distance is less than 3.05 Å for H···S and 2.60 Å for H···O.

Table 3 The assignments of the observed vibrational frequencies (cm^{-1}) of ME in the S–H stretching region

Conformers		υ_{obs}	υ_{cal}	Raman activity[a]
1	GGg	2587	2587	116
2	G′Gg	2601	2603	106
3	G′Gt	2604	2609	98
4	G′Gg′		2600	99
5	G′Tt	2593	2593	116
6	G′Tg	2593	2595	118
7	G′Tg′	2593	2592	115
8	TTt		2612	147
9	TTg′		2613	146
10	G′G′t		2599	118

[a] Calculated at B3LYP-D3(BJ)/aug-cc-PVDZ.

orientations of the functional group correspond to different vibrational frequencies, and on the other hand, the S–H···O interaction is indeed weak, as indicated by the calculated H···O distance, which is only 0.01 A shorter than the sum of the van der Waals radii of H and O atoms in conformer 3. Such a weak interaction is insufficient to induce an observable red shift, suggesting very weak S–H···O intramolecular interactions in the gaseous ME molecule. In a recent rotational spectroscopic investigation on gas-phase 2-phenylethanethiol, it was shown that the global minimum was the result of intramolecular forces associated with an S–H···π H-bond despite the weak character of the S serving as the H-bond donor.[32]

Molecular conformational equilibrium is strongly temperature-dependent *via* the Gibbs free energy. To further validate spectral assignments, we measured the temperature-dependent S–H stretching Raman spectra of ME at 25, 35, 45, 55, and 65 °C, as shown in Fig. 3. All spectral intensities were normalized relative to the strongest peak at 2587 cm^{-1}. In contrast to the band at 2587 cm^{-1}, the relative intensities of the 2593 and 2601 cm^{-1} bands increased as the temperature increased, indicating that the 2587 cm^{-1} peak corresponds to the most stable conformer of GGg, in good agreement with theoretical prediction. In addition, the shoulder at 2604 cm^{-1} becomes less distinct due to band broadening at high temperatures of 55 and 65 °C.

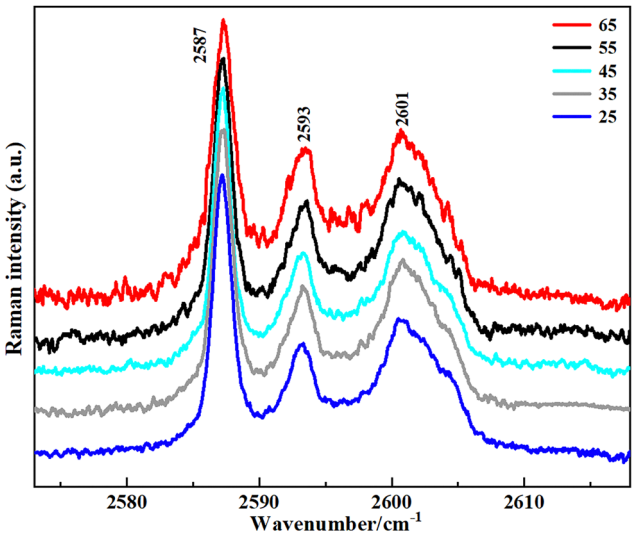

Fig. 3 Temperature-dependent Raman spectra of the gaseous ME in the S–H stretching region at 25, 35, 45, 55 and 65 °C.

3.3 Intermolecular hydrogen bonds in the liquid state

Fig. 4(a) shows the Raman spectra of ME in the S–H stretching region for the pure liquid state and for an aqueous solution with a mole fraction of ME at 0.2. Unlike the well-separated bands observed in the gas-phase spectra, the liquid-phase spectra broadened into a single band due to intermolecular interactions, which prevents conformational discrimination. On the other hand, the band center of the S–H stretching vibration shifts from 2580 cm^{-1} in aqueous solution to 2574 cm^{-1} in the pure liquid, corresponding to a red-shift of about 6 cm^{-1}. It is known that molecular clusters serve as a bridge that connects molecules in the gas phase and in the condensed phase, thereby providing molecular-level insight into intermolecular interactions and microscopic structures in the liquid state.[29] To uncover the origin of the observed red shift, quantum-chemical calculations were performed on dimers formed between ME molecules (labeled ME-ME) and between ME and a water molecule (labeled ME–H_2O).

Fig. 4(b) shows the calculated most stable structures of the ME–ME and ME–H_2O dimers at the B3LYP-D3(BJ)/aug-cc-PVDZ level, and a scaling factor of 0.978 was applied for the calculated harmonic frequency like the ME monomer. Both dimers exhibit a cooperative H-bonded network connected by O–H···O, O–H···S, or S–H···O interactions, and their structural parameters are summarized in Table 2. As expected, the H-bond strength follows the order O–H···O > O–H···S > S–H···O, based on the deviation (Δ) between the H-bond distance and the sum of the van der Waals radii. However, unlike the extremely weak intramolecular interaction in the monomers, the S–H···O intermolecular hydrogen bond is markedly enhanced in the ME-ME dimer. As shown in Table 2, the S–H···O distance is 0.39 Å shorter than the sum of the van der Waals radii of H and O atoms, representing an increase of 0.38 Å compared with the intramolecular value of 0.01 Å. In contrast, the ME–H_2O dimer is linked only by O–H···O and O–H···S interactions. Clearly, the formation of the S–H···O intermolecular hydrogen bond in the ME-ME dimer causes a red-shift of the S–H stretching frequency relative to that in the ME–H_2O dimer, as illustrated by their calculated frequencies in Fig. 4(a), where the calculated S–H stretching frequencies are 2564 and 2600 cm^{-1} for the ME-ME dimer and 2599 cm^{-1} for ME–H_2O. Thus, the experimentally observed red-shift provides evidence for the formation of S–H···O interactions in neat liquid ME, indicating that sulfur can act as a much more effective donor in intermolecular H-bonding interactions in

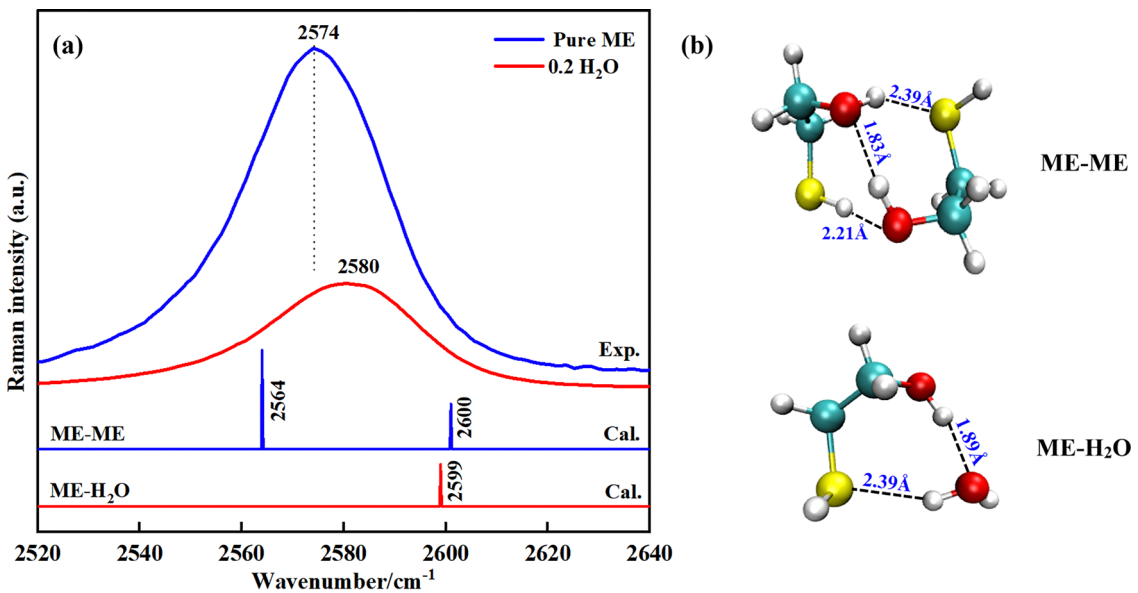

Fig. 4 (a) S–H stretching Raman spectra of pure liquid ME and its solution in water with a molar fraction of ME at 0.2, along with the calculated frequencies for ME-ME and ME–H_2O dimers. (b) Calculated H-bonded structures of the ME–ME and ME–H_2O dimers.

the liquid state. This finding is in agreement with recent studies on 1:1 complexes of 2-fluorothiophenol (2-FTP) with methanol (MeOH) and ethanol (EtOH) under jet-cooled conditions employing resonant two-photon ionization, UV–UV hole-burning, and IR–UV double resonance spectroscopic techniques, showing that all the observed conformers of the two complexes are primarily S–H···O hydrogen bonded.[26]

4. Conclusion

Raman spectroscopy combined with high-level quantum chemical calculations provides a synergistic approach for characterizing molecular structures as well as intramolecular and intermolecular interactions. In this work, sulfur-centered H-bonding interactions in gaseous and liquid mercaptoethanol (ME) have been systematically investigated using temperature-dependent Raman spectroscopy combined with quantum chemical calculations. High-resolution gas-phase Raman spectra in the S–H stretching region were successfully recorded, despite the intrinsically weak Raman cross-section and low vapor pressure, enabling the identification of individual conformers and relating their relative stability to the O–H···S and S–H···O intramolecular H-bond strengths. It was shown that both intramolecular H-bonds played an important role in stabilizing ME conformers in the gas phase, but the S–H···O interaction is extremely weak and insufficient to induce an observable red shift in the S–H stretching frequency. In contrast, Raman measurements in the liquid phase revealed a clear red shift of the S–H stretching band in neat ME relative to the aqueous solution. Supported by the calculated structural parameters on the ME–ME and ME–H_2O dimers, the red shift is attributed to the formation of a significantly strengthened S–H···O intermolecular H-bond in the liquid state, facilitated by favorable spatial arrangements and cooperative hydrogen-bonding networks. These results provide direct spectroscopic evidence for the environment-dependent nature of sulfur-centered hydrogen bonding and contribute to a deeper understanding of the competition and synergy between sulfur-centered intra- and intermolecular interactions, which may be useful across various research fields, including protein folding, molecular aggregation, and computational benchmarking.[1–51]

Author contributions

Siyao Li: data curation (equal); formal analysis (equal); investigation (equal); visualization (equal). Yuhui Li: data curation (equal); methodology (equal). Xinlang Yang: data curation (equal). Yuanqin Yu: conceptualization (lead); funding acquisition (equal); supervision (lead); writing – original draft (lead); writing – review & editing (equal). Xiaoguo Zhou: conceptualization (supporting); writing – original draft (supporting). Rui Zhang: funding acquisition (equal); writing – review & editing (supporting). Jinsong Li: writing – review & editing (supporting). Shilin Liu: funding acquisition (equal); resources (lead).

Conflicts of interest

There are no conflicts of interest to declare

Data availability

The authors confirm that the data supporting the findings of this study are available within the article.

Acknowledgements

This work was supported by the National Natural Science Foundation of China (Grants No. 21873002, 22027801 and 12374001).

References

1 G. A. Jeffrey and W. Saenger, *Hydrogen bonding in biological structures*, Springer Science & Business Media, 1990.
2 G. R. Desiraju, *The Weak Hydrogen Bond: In Structural Chemistry and Biology*, Oxford University Press, Oxford, New York, 1999.
3 B. K. Paul, N...H-N versus O...H-N intramolecular hydrogen bonding in E- and Z-isomers of para-substituted phenylhydrazones: Differential nature of the H-bonds and the exception of para-CN substituent, *Comput. Theor. Chem.*, 2024, **1231**, 114413.
4 F. Meemken, N. Maeda, K. Hungerbühler and A. Baiker, Platinum-Catalyzed Asymmetric Hydrogenation: Spectroscopic Evidence for an O–H–O Hydrogen-Bond Interaction between Substrate and Modifier, *Angew. Chem., Int. Ed.*, 2012, **51**(33), 8212–8216.
5 P. Barczynski, Z. Dega-Szafran, A. Katrusiak and M. Szafran, O–H···O and O–H···N hydrogen bonds in the complex of DABCO mono-betaine with p-hydroxybenzoic acid studied by X-ray diffraction, DFT calculations and spectroscopic methods, *J. Mol. Struct.*, 2011, **1000**(1–3), 127–134.
6 Y. Katsumoto, T. Tanaka, K. Ihara, M. Koyama and Y. Ozaki, Contribution of intramolecular C = O...H-N hydrogen bonding to the solvent-induced Reentrant phase separation of Poly(N-isopropylacrylamide), *J. Phys. Chem. B*, 2007, **111**(44), 12730–12737.
7 K. C. K. Swamy, S. Kumaraswamy and P. Kommana, Very strong C–H···O, N-H···O, and O-H···O hydrogen bonds involving a cyclic phosphate, *J. Am. Chem. Soc.*, 2001, **123**(50), 12642–12649.
8 Y. Q. Yu, W. Fan, Y. X. Wang, X. G. Zhou, J. Sun and S. L. Liu, C–H···O Interaction in Methanol-Water Solution Revealed from Raman Spectroscopy and Theoretical Calculations, *J. Phys. Chem. B*, 2017, **121**(34), 8179–8187.
9 A. Singh, K. Avinash, A. K. Pradhan, A. K. Prajapati, A. J. Edwards and S. P. Thomas, Weak yet directional: supramolecular interactions of thiols unravelled by quantum crystallography, *Chem. Sci.*, 2025, **16**(35), 16016–16026.
10 H. S. Biswal, S. Bhattacharyya, A. Bhattacherjee and S. Wategaonkar, Nature and strength of sulfur-centred hydrogen bonds: laser spectroscopic investigations in the

gas phase and quantum-chemical calculations, *Int. Rev. Phys. Chem.*, 2015, **34**(1), 99–160.

11 E. Gross, C. S. Sevier, N. Heldman, E. Vitu, M. Bentzur, C. A. Kaiser, C. Thorpe and D. Fass, Generating disulfides enzymatically: Reaction products and electron acceptors of the endoplasmic reticulum thiol oxidase Ero1p, *Proc. Natl. Acad. Sci. USA*, 2006, **103**(2), 299–304.

12 D. Fass and C. Thorpe, Chemistry and Enzymology of Disulfide Cross-Linking in Proteins, *Chem. Rev.*, 2018, **118**(3), 293–322.

13 L. T. Wang, W. Q. Li, Y. G. Xu, F. Shen, W. Caminati, A. Lesarri and G. Feng, The sulfur lone-pair···π interaction: The subtle dispersion features of the sulfur interactions in model complexes of disulfides with the heteroaromatic benzofuran, *J. Chem. Phys.*, 2025, **163**(2), 024302.

14 W. Fan, L. Xing, N. Chen, X. G. Zhou, Y. Q. Yu and S. L. Liu, Promotion Effect of Succinimide on Amyloid Fibrillation of Hen Egg-White Lysozyme, *J. Phys. Chem. B*, 2019, **123**(38), 8057–8064.

15 F. Shen, L. T. Wang, R. H. Chen, W. Q. Li, Y. T. Li, Y. Feng, T. Lu, W. Caminati, A. Lesarri and G. Feng, Unraveling the S-S···π interactions in furan-disulfide heterodimers: insights from microwave spectroscopy and ab initio computations, *Phys. Chem. Chem. Phys.*, 2025, **27**(38), 20802–20809.

16 P. Samanta and P. Banerjee, Modulations in the binding selectivity of phenol and thiophenol with ethyl cinnamate: an IR spectroscopic and quantum chemical investigation, *Phys. Chem. Chem. Phys.*, 2025, **27**(36), 19170–19180.

17 A. K. Sahu, A. R. Satpathi, S. Rout, R. Samanta, L. Dash and H. S. Biswal, Disulfide-Centered Hydrogen Bonding: Insights from Protein Structure Analysis and IR-UV Double Resonance Spectroscopy, *J. Phys. Chem. Lett.*, 2025, **16**(40), 10455–10465.

18 P. Pinacho, C. Pérez, M. Stahn, R. T. Saragi, A. Hansen, S. Grimme, A. Lesarri and M. Schnell, Hydrogen Bond Interaction Networks in the Mixed Pentamers of Hydrogen Sulfide and Water, *J. Am. Chem. Soc.*, 2025, **147**(22), 18576–18582.

19 X. L. Li, W. Q. Lv, J. U. Grabow and G. Feng, Exploring the intra- and intermolecular disulfide-centered non-covalent interactions in methyl allyl disulfide and its complex with water, *J. Chem. Phys.*, 2025, **163**(19), 194302.

20 F. Torres-Hernández, P. Pinillos, W. Q. Li, R. T. Saragi, A. Camiruaga, M. Juanes, I. Usabiaga, A. Lesarri and J. A. Fernández, Competition between O-H and S-H Intermolecular Interactions in Conformationally Complex Systems: The 2-Phenylethanethiol and 2-Phenylethanol Dimers, *J. Phys. Chem. Lett.*, 2024, **15**(21), 5674–5680.

21 W. Silva, T. Poonia and J. van Wijngaarden, Exploring the conformational landscape, hydrogen bonding, and internal dynamics in the diallyl ether and diallyl sulfide monohydrates, *J. Chem. Phys.*, 2024, **160**(4), 044302.

22 H. Y. Shen, N. Chen, A. You, Y. Q. Yu, X. G. Zhou, R. Zhang and S. L. Liu, Structural features of liquid DMSO from temperature-dependent Raman spectroscopy and theoretical calculations, *Chin. J. Chem. Phys*, 2024, **37**(6), 763–768.

23 W. Q. Lv, Y. G. Xu, T. T. Yang, L. T. Wang, J. X. Huang, H. Y. Huang and G. Feng, Unveiling the underappreciated: The bonding features of C-H···S-S interactions observed from rotational spectroscopy, *J. Chem. Phys.*, 2024, **160**(13), 134302.

24 B. K. Oram, Monu, A. Kothari and B. Bandyopadhyay, Competition between C–H···S and S–H···Cl H-bonds in a $CHCl_3$-H_2S complex: a combined matrix isolation IR spectroscopic and quantum chemical investigation, *Phys. Chem. Chem. Phys.*, 2024, **27**(1), 564–576.

25 P. Meyer, S. Jäger, J. Khatri, S. Henkel, G. Schwaab and M. Havenith, Mixed H2S and H2O Clusters-New Insights into Dispersion-Dominated Hydrogen Bonding, *J. Phys. Chem. A*, 2024, **128**(44), 9627–9633.

26 S. Metya, S. Roy, S. Mandal, Q. R. Huang, J. L. Kuo and A. Das, Modulation of the strength of weak S-H···O hydrogen-bond: Spectroscopic study of the complexes of 2-flurothiophenol with methanol and ethanol, *J. Chem. Phys.*, 2024, **160**(22), 224302.

27 W. Q. Lv, J. X. Huang, H. Y. Huang, L. T. Wang, T. T. Yang and G. Feng, The C–H···S–S hydrogen bonding in diethyl disulfide···difluoromethane: a combined microwave spectroscopic and computational study, *Phys. Chem. Chem. Phys.*, 2024, **26**(48), 29940–29947.

28 P. Bhadoria and V. Ramanathan, Combined FTIR/Raman spectroscopic studies and ab initio electronic structure calculations of Dithiothreitol, *Spectrochim. Acta, Part A*, 2024, **304**, 123399.

29 M. K. Tripathi and V. Ramanathan, Nature and Strength of Sulfur-Centered Hydrogen Bond in Methanethiol Aqueous Solutions, *J. Phys. Chem.A*, 2023, **127**(10), 2265–2273.

30 T. Lu, J. Q. Zhang, Y. G. Xu, Z. Wang, G. Feng and Z. Zeng, Hydrogen bond interactions between thioethers and amides: A joint rotational spectroscopic and theoretical study of the formamide…dimethyl sulfide adduct, *Spectrochim. Acta, Part A*, 2023, **288**, 122199.

31 P. Bhadoria and V. Ramanathan, Sulfur Centered Hydrogen Bonding in Thioglycolic Acid and Its Clusters: A Computational Exploration, *J. Phys. Chem. A*, 2023, **127**(39), 8095–8109.

32 R. T. Saragi, W. Q. Li, M. Juanes, L. Enríquez, R. Pinacho, J. E. Rubio and A. Lesarri, Rotational Spectroscopy and Conformational Flexibility of 2-Phenylethanethiol: The Dominant S-H···π Intramolecular Hydrogen Bond, *Chem. Phys. Chem.*, 2024, **25**(5), e202300799.

33 A. Paul and R. Thomas, Evidences for sulfur centered hydrogen bond with sulfur atoms as a donor in aromatic thiols and aliphatic thiols in aqueous solution, *J. Mol. Liq.*, 2022, **348**, 118078.

34 B. Hartwig and M. A. Suhm, Subtle hydrogen bonds: benchmarking with OH stretching fundamentals of vicinal diols in the gas phase, *Phys. Chem. Chem. Phys.*, 2021, **23**(38), 21623–21640.

35 Y. Q. Yu, Y. X. Wang, K. Lin, X. G. Zhou, S. L. Liu and J. Sun, New spectral assignment of n-propanol in the C-H stretching region, *J. Raman Spectrosc.*, 2016, **47**(11), 1385–1393.

36 Y. Q. Yu, Y. X. Wang, N. Y. Hu, K. Lin, X. G. Zhou and S. L. Liu, Cβ-H stretching vibration as a new probe for conformation of n-propanol in gaseous and liquid states, *Phys. Chem. Chem. Phys.*, 2016, **18**(15), 10563–10572.

37 Y. Q. Yu, Y. X. Wang, K. Lin, N. Y. Hu, X. G. Zhou and S. L. Liu, Complete Raman Spectral Assignment of

Methanol in the C-H Stretching Region, *J. Phys. Chem. A*, 2013, **117**(21), 4377–4384.

38 D. L. Thomsen, J. L. Axson, S. D. Schroder, J. R. Lane, V. Vaida and H. G. Kjaergaard, Intramolecular Interactions in 2-Aminoethanol and 3-Aminopropanol, *J. Phys. Chem. A*, 2013, **117**(40), 10260–10273.

39 Y. H. Li, X. L. Yang, Y. Q. Yu, X. G. Zhou, R. Zhang, J. Sun and S. L. Liu, Dependence of Intramolecular Hydrogen Bond on Conformational Flexibility in Linear Aminoalcohols, *J. Phys. Chem. A*, 2023, **127**(43), 9013–9021.

40 A. You, Y. H. Li, X. L. Yang, H. Y. Shen, Y. Q. Yu, X. G. Zhou, R. Zhang and S. L. Liu, Conformational equilibrium of aminoethanol in the gas phase and in solution driven by intra- and intermolecular interactions and solvent polarity, *J. Chem. Phys.*, 2025, **162**(16), 164309.

41 S. Eun-Mo and M. D. Harmony, The Microwave Spectrum, Structure, and Dipole Moment of 2-Mercaptoethanol; Evidence for an Intramolecular OH-S Hydrogen Bond, *J. Am. Chem. Soc.*, 1977, **99**(17), 5603–5608.

42 B. J. Miller, M. Yekutiel, A. H. Sodergren, D. L. Howard, M. E. Dunn, V. Vaida and H. G. Kjaergaard, Overtone Spectra of 2-Mercaptoethanol and 1,2-Ethanedithiol, *J. Phys. Chem. A*, 2010, **114**(48), 12692–12700.

43 S. K. Nandy, D. K. Mukherjee, S. B. Roy and G. S. Kastha, Vibrational Spectra and Rotational Isomerism in 2-Mercaptoethanol, *Can. J. Chem.*, 1973, **51**(7), 1139–1141.

44 T. Li, W. Fan, J. Sun, Y. Q. Yu, X. G. Zhou, C. M. Xie and S. L. Liu, The role of weak C-H···O hydrogen bond in alcohol-water mixtures, *J. Raman Spectrosc.*, 2022, **53**(9), 1551–1559.

45 R. Kobayashi, J. Normand, K. Raghavachari, A. P. Rendell, J. C. Burant, S. S. Iyengar, J. Tomasi, M. Cossi, J. M. Millam, M. Klene, *et al. Gaussian 16 Rev. C.01.*, Wallingford, CT, 2016.

46 Tian, L. Molclus Program, Version 1.3.5., 2016, https://www.keinsci.com/research/molclus.html.

47 W. H. Sun, O. P. Sogeke, W. Silva and J. van Wijngaarden, Dispersion-driven conformational preference in the gas phase: Microwave spectroscopic and theoretical study of allyl isocyanate, *J. Chem. Phys.*, 2019, **151**(19), 194304.

48 T. Lu and Q. Chen, Shermo: A general code for calculating molecular thermochemistry properties, *Comput. Theor. Chem.*, 2021, **1200**, 113249.

49 R. Chaudret, B. de Courcy, J. Contreras-García, E. Gloaguen, A. Zehnacker-Rentien, M. Mons and J. P. Piquemal, Unraveling non-covalent interactions within flexible biomolecules: from electron density topology to gas phase spectroscopy, *Phys. Chem. Chem. Phys.*, 2014, **16**(21), 9876–9891.

50 T. Lu and F. Chen, Multiwfn: A Multifunctional Wavefunction Analyzer, *J. Comput. Chem.*, 2012, **33**, 580–592.

51 K. K. Mishra, K. Borish, G. Singh, P. Panwaria, S. Metya, M. S. Madhusudhan and A. Das, Observation of an Unusually Large IR Red-Shift in an Unconventional S-H3···S Hydrogen-Bond, *J. Phys. Chem. Lett.*, 2021, **12**(4), 1228–1235.